1992ApJ...390..378J

THE ASTROPHYSICAL JOURNAL, 390:378–386, 1992 May 10
© 1992. The American Astronomical Society. All rights reserved. Printed in U.S.A.

SWING AMPLIFICATION OF NONAXISYMMETRIC PERTURBATIONS IN STARS AND GAS IN A SHEARED GALACTIC DISK

CHANDA J. JOG
Department of Physics, Indian Institute of Science, Bangalore 560012, India
Received 1991 May 14; accepted 1991 November 6

ABSTRACT

We present a study of the growth of local, nonaxisymmetric perturbations in gravitationally coupled stars and gas in a differentially rotating galactic disk. The stars and gas are treated as two isothermal fluids of different velocity dispersions, with the stellar velocity dispersion being greater than that for the gas. We examine the physical effects of inclusion of a low-velocity dispersion component (gas) on the growth of nonaxisymmetric perturbations in both stars and gas, as done for the axisymmetric case by Jog & Solomon. The amplified perturbations in stars and gas constitute trailing, material, spiral features which may be identified with the local spiral features seen in all spiral galaxies.

The formulation of the two-fluid equations closely follows the one-fluid treatment by Goldreich & Lynden-Bell. The local, linearized perturbation equations in the sheared frame are solved to obtain the results for a temporary growth via swing amplification. The problem is formulated in terms of five dimensionless parameters—namely, the Q-factors for stars and gas, respectively; the gas mass fraction; the shearing rate in the galactic disk; and the length scale of perturbation. By using the observed values of these parameters, we obtain the amplifications and the pitch angles for features in stars and gas for dynamically distinct cases, as applicable for different regions of spiral galaxies.

A real galaxy consisting of stars and gas may display growth of nonaxisymmetric perturbations even when it is stable against axisymmetric perturbations and/or when either fluid by itself is stable against nonaxisymmetric perturbations.

Due to its lower velocity dispersion, the gas exhibits a higher amplification than do the stars, and the amplified gas features are slightly more tightly wound than the stellar features. When the gas contribution is high, the stellar amplification and the range of pitch angles over which it can occur are both increased, due to the gravitational coupling between the two fluids. Thus, the two-fluid scheme can explain *the origin of the broad spiral arms in the underlying old stellar populations* of galaxies, as observed by Schweizer and Elmegreen & Elmegreen. The arms are predicted to be broader in gas-rich galaxies, as is indeed seen for example in M33. In the linear regime studied here, *the arm contrast is shown to increase with radius in the inner Galaxy*, in agreement with observations of external galaxies by Schweizer. These results follow directly due to the inclusion of gas in the problem.

Subject headings: galaxies: ISM — galaxies: kinematics and dynamics — galaxies: spiral — hydrodynamics — instabilities

1. INTRODUCTION

An analysis of local, axisymmetric instabilities in a galactic disk consisting of stars and gas was presented by Jog & Solomon (1984a, b, hereafter JS1 and JS2 respectively). In that work, a galactic disk is treated as a two-fluid system where stars and gas are taken to be two isothermal fluids with different velocity dispersions, with the stellar velocity dispersion being greater than that in the gas. The two fluids interact gravitationally with each other. The existence of even a small fraction ($\leq$10%–20%) of the total disk density in a low-velocity dispersion component, namely gas, was shown to significantly decrease the stability of the entire two-fluid disk.

In a two-dimensional disk, the general perturbation is nonaxisymmetric. Because of the differential rotation in a galactic disk, this case is not a trivial extension of the axisymmetric case. The epicyclic motion of a disk particle and the local, unperturbed shear flow in a sheared galactic disk have a similar sense of motion. This, plus the self-gravity of the fluid, leads to a strong though temporary growth of the nonaxisymmetric perturbations even when the disk is stable to the growth of axisymmetric perturbations. This was shown for a one-component case—for gas by Goldreich & Lynden-Bell (1965, hereafter GLB), and for stars by Julian & Toomre (1966)—who also indentified the amplified, local, nonaxisymmetric perturbations with local spiral features in spiral galaxies. Toomre (1981) has called this phenomenon *swing amplification* since the maximum growth occurs as a wave swings from a radial to a trailing position.

These one-fluid results have been confirmed through numerical simulation work by Sellwood & Carlberg (1984) and Carlberg & Freedman (1985). They have also shown that gas accretion onto a galaxy and/or star formation, or cloud collisions, lead to an effective dynamical cooling of the disk, and hence allow the formation and growth of recurring spiral features. However, the cooling of the disk is introduced in an ad hoc fashion in these papers.

In the present paper, we study the growth of local, nonaxisymmetric perturbations leading to swing amplification, in the coupled stars and gas in a two-fluid galactic disk. The aim is to study *the physical effects of inclusion of gas* on the growth of perturbations in both stars and gas in a galaxy. By the appropriate choice of observed values for the five dimension-

© American Astronomical Society • Provided by the NASA Astrophysics Data System

1992ApJ...390..378J

less parameters in the problem, we obtain the two-fluid amplification results as applicable to different regions and types of spiral galaxies.

The lower velocity component, namely the gas, shows a higher amplification than the stars, and the gas features are more tightly wound than the stellar ones. When the gas contribution is high, the stellar amplification and the range of pitch angles over which it occurs are increased, due to the coupling between the two fluids. Thus we can explain the origin of the broad spiral arms in the old stellar populations as observed by Schweizer (1976), and Elmegreen & Elmegreen (1984). The arm contrast in the inner Galaxy is shown to increase with radius, this agrees with observations of external galaxies by Schweizer (1976).

We thus explain the local spiral features in all spiral galaxies as being trailing, material arms which arise as the amplified, local, nonaxisymmetric perturbations in stars and gas. Our analysis is particularly applicable to galaxies which exhibit a patchy or messy spiral structure with many, fragmented spiral arms, such as M33 (NGC 598), or NGC 2841, or NGC 488. Such galaxies are more common than the grand-design spiral galaxies, such as M51 (NGC 5194) (e.g., Binney & Tremaine 1987).

The coupled, linearized equations governing the growth of nonaxisymmetric perturbations in a sheared, two-fluid galactic disk are obtained in § 2. These are solved as an initial value problem, and results are obtained for realistic values of parameters (§ 3). Section 4 contains a summary of conclusions from this paper.

2. NONAXISYMMETRIC PERTURBATIONS IN STARS AND GAS

2.1. *Physical Parameters of a Two-Fluid Galactic Disk*

We assume that the stars and the gas in the disk form two isothermal fluids, each characterized by μ_i, the surface density, and c_i, the isothermal sound speed or the one-dimensional rms velocity dispersion in the fluid. The subscripts $i = s$ and g denote the parameters for the stars and gas, respectively. The gas fluid is "colder," that is, $c_g \ll c_s$. The two fluids interact gravitationally with each other. They are distributed geometrically in an infinitesimally thin disk which is supported by the differential rotation and the random motion of the fluids. The two fluids corotate with each other. The unperturbed and perturbed surface density and gravitational potential are denoted by μ_0, $\delta\mu$ and ψ_0, $\delta\psi$, respectively.

The fluid representation of stars as used here simplifies the mathematical treatment. Though not completely rigorous, it is still physically relevant for the local, linear analysis of the nonaxisymmetric perturbations (e.g., Goldreich & Tremaine 1978), and in regions away from the Lindblad resonance (Bertin 1980) and for moderately sheared features (Julian & Toomre 1966)—which correspond to the range of maximum amplifications as we will show in § 3.

2.2. *Formulation of Equations*

We consider local perturbations—that is, those with wavelengths small compared to the galactocentric radial distance. The perturbations are taken to be planar—this requires the minimum wavelength of perturbation to be greater than the vertical scale height of the stars (> the scale height of the gas). The formulation of the hydrodynamic equations closely follows the one-fluid treatment by GLB, except that we treat a two-fluid system, and also we consider an infinitesimally thin disk whereas GLB treat a finite height disk. The thin disk assumption simplifies the calculation and still gives reasonably accurate results (to within $\leq 15\%$), as shown for the axisymmetric case (Toomre 1964; JS1).

In the following analysis the subscripts $i = s$ and $i = g$ describe the equations for star and gas, respectively. The Euler equations in a uniformly rotating frame (using galactocentric cylindrical coordinates r, ϕ, z) are given as

$$\frac{\partial \boldsymbol{V}_i}{\partial t} + (\boldsymbol{V}_i \cdot \nabla)\boldsymbol{V}_i = -\frac{c_i^2}{\mu_{0i}}\nabla\mu_i - \nabla(\psi_s + \psi_g) - 2\boldsymbol{\Omega} \times \boldsymbol{V}_i + \Omega^2 \boldsymbol{r} \quad (1), (2)$$

where $\boldsymbol{\Omega} = \Omega \boldsymbol{z}$ is the angular velocity of the rotating frame. $\Omega = -\Omega_0$ where Ω_0 is the rotation of the disk as in the standard notation; this choice is suitable since we want to study the growth of trailing features. Note that $B - A = -\Omega_0 = \Omega$ where A and B are the standard Oort constants. $\boldsymbol{V}_i$ denotes the two-dimensional fluid velocity with respect to the rotating axes. The right-hand sides of equations (1) and (2) denote the force experienced by either fluid in the rotating frame. Note that because of the gravitational interaction between stars and gas, each fluid experiences the joint gravitational potential, $(\psi_s + \psi_g)$, resulting from the two fluids.

Consider a point (r_0, ϕ_0) that is corotating in the above rotating frame. We study the dynamics of the local region around this point. Consider Cartesian axes (x, y, z) centered at the origin (r_0, ϕ_0), with unit vectors $\boldsymbol{i}, \boldsymbol{j}, \boldsymbol{k}$ respectively, with $\boldsymbol{i}$ along the initial outward radial direction. The unperturbed velocities $\boldsymbol{V}_{0i}$ of the sheared flow in the galactic disk, with respect to these axes, are given as (see GLB) follows:

$$\boldsymbol{V}_{0s} = \boldsymbol{V}_{0g} = 2Ax\boldsymbol{j}\,. \quad (3)$$

The associated coriolis term in equations (1)–(2), $(= 4A\Omega_0 x\boldsymbol{i})$, is assumed to be balanced by the unperturbed gravitational force $[= -\nabla(\psi_{0s} + \psi_{0g})]$ as in GLB. Let v_{xi} and v_{yi} denote the perturbation velocity components. Hence the Euler equations for local, linear perturbations in stars and gas are

$$\frac{\partial v_{xi}}{\partial t} + 2Ax\frac{\partial v_{xi}}{\partial y} - 2\Omega v_{yi} = -\frac{\partial}{\partial x}(\delta\psi_s + \delta\psi_g) - \frac{c_i^2}{\mu_{0i}}\frac{\partial(\delta\mu_i)}{\partial x} \quad (4), (5)$$

$$\frac{\partial v_{yi}}{\partial t} + 2Ax\frac{\partial v_{yi}}{\partial y} + 2Bv_{xi} = -\frac{\partial}{\partial y}(\delta\psi_s + \delta\psi_g) - \frac{c_i^2}{\mu_{0i}}\frac{\partial(\delta\mu_i)}{\partial y}\,. \quad (6), (7)$$

Similarly, the linear perturbation equations for the equations of continuity, and the joint Poisson equation for an infinitesimally thin disk are

$$\frac{\partial(\delta\mu_i)}{\partial t} + 2Ax\frac{\partial(\delta\mu_i)}{\partial y} + \mu_{0i}\left(\frac{\partial v_{xi}}{\partial x} + \frac{\partial v_{yi}}{\partial y}\right) = 0 \quad (8), (9)$$

$$\left(\frac{\partial^2}{\partial x^2} + \frac{\partial^2}{\partial y^2} + \frac{\partial^2}{\partial z^2}\right)(\delta\psi_s + \delta\psi_g) = 4\pi G(\delta\mu_s + \delta\mu_g)\delta(z)\,, \quad (10)$$

where $\delta(z)$ is the Dirac delta function.

We next introduce sheared axes which are comoving with the unperturbed flow in the above uniformly rotating frame—this is the natural choice for the study of sheared modes. The sheared coordinates are defined as x', y', z', t', where

$$x' = x\,, \quad y' = y - 2Axt\,, \quad z' = z\,, \quad \text{and } t' = t \quad (11)$$

© American Astronomical Society • Provided by the NASA Astrophysics Data System

1992ApJ...390..378J

so that

$$\left[\frac{\partial}{\partial x}=\frac{\partial}{\partial x'}-2At'\frac{\partial}{\partial y'}\right],\quad \frac{\partial}{\partial y}=\frac{\partial}{\partial y'},\quad \frac{\partial}{\partial z}=\frac{\partial}{\partial z'},$$

and (12)

$$\left[\frac{\partial}{\partial t}=\frac{\partial}{\partial t'}-2Ax'\frac{\partial}{\partial y'}\right].$$

It is easy to see that the linearized fluid equations (eqs. [4]–[10]) when written in terms of the sheared coordinates allow Fourier analysis in x' and y', but not in t' since these equations contain terms proportional to t'. Therefore, the trial solution for the independent variables may be taken to be proportional to $\exp[i(k_x x' + k_y y')]$, and the magnitudes for the parameters v_{xi}, v_{yi}, $\delta\mu_i$, $\delta\psi_i$ are denoted by the respective quantities (v_{xi}, etc.). These equations are solved to obtain $\delta\mu_s$ and $\delta\mu_g$ as functions of time given their initial values. Next, following GLB, define τ (for a wavenumber $k_y \neq 0$):

$$\tau \equiv 2At' - k_x/k_y . \tag{13}$$

In the sheared frame, τ is a dimensionless measure of time t', and it has different zeroes for each mode with a different k_x/k_y. In each case, $\tau = 0$ when the wavefront is along $\boldsymbol{i}$ (along the radial direction), that is when the wavevector is along $\boldsymbol{j}$ as can be seen by transforming the trial solution back to the nonsheared frame

$$\exp i(k_x x' + k_y y') = \exp i[k_y(-\tau x + y)] . \tag{14}$$

Note that the wavenumber is constant with τ in the sheared frame while in the uniformly rotating frame it increases with τ ($k_{\text{nonsheared}} = k_y[1+\tau^2]^{1/2} = k_y \sec\gamma$). Here $\tan\gamma = \tau$ and γ is the (pitch) angle between the instantaneous wavefront and $\boldsymbol{i}$. Hence $\delta\mu_i(\tau)$ represents the density variation with time in the sheared frame; whereas, in the nonsheared frame, it gives the density for a mode of wavenumber $[k_y(1+\tau^2)^{1/2}]$ that is sheared by an angle $\gamma = \tan^{-1}\tau$ with respect to $\boldsymbol{i}$. The larger the value of τ, the more tightly wound is the perturbation.

Thus, the local, linearized perturbation equations (4)–(10) can be written in terms of the sheared coordinates using equations (11)–(12); and with the trial solution as described above and with the above definition of τ, these reduce to

$$\frac{\partial v_{xi}}{\partial\tau}-\frac{\Omega}{A}v_{yi} = -i\frac{k_y}{2A}\tau\left[-(\delta\psi_s+\delta\psi_g)-\frac{c_i^2}{\mu_{0i}}(\delta\mu_i)\right] \tag{15), (16}$$

$$\frac{\partial v_{yi}}{\partial\tau}+\frac{B}{A}v_{xi} = i\frac{k_y}{2A}\left[-(\delta\psi_s+\delta\psi_g)-\frac{c_i^2}{\mu_{0i}}(\delta\mu_i)\right]. \tag{17), (18}$$

$$\frac{\partial}{\partial\tau}(\delta\mu_i) - i\frac{k_y}{2A}\tau\mu_{0i}v_{xi} + i\frac{k_y}{2A}\mu_{0i}v_{yi} = 0 \tag{19), (20}$$

$$\left[-k_y^2(1+\tau^2)+\frac{\partial'^2}{\partial z^2}\right](\delta\psi_s+\delta\psi_g) = 4\pi G(\delta\mu_s+\delta\mu_g)\delta(z') . \tag{21}$$

Now, the Poisson equation (eq. [21]) can be solved easily, and it gives

$$(\delta\psi_s+\delta\psi_g) = -\left[\frac{2\pi G}{k_y(1+\tau^2)^{1/2}}\right](\delta\mu_s+\delta\mu_g) . \tag{22}$$

Next, define θ_i, the dimensionless perturbation surface density, to be the ratio of the perturbation surface density to the unperturbed surface density:

$$\theta_i \equiv \delta\mu_i/\mu_{0i} . \tag{23), (24}$$

Substituting equations (22)–(24) back into equations (15)–(20), and assuming nonvortical perturbations as in GLB, we obtain the following two coupled equations which describe the evolution with τ in θ_i:

$$\left(\frac{d^2\theta_i}{d\tau^2}\right)-\left(\frac{d\theta_i}{d\tau}\right)\left(\frac{2\tau}{1+\tau^2}\right)+\theta_i\left[\frac{\kappa^2}{4A^2}+\frac{2B/A}{1+\tau^2}+\frac{k_y^2}{4A^2}(1+\tau^2)c_i^2\right]$$
$$= (\mu_{0s}\theta_s+\mu_{0g}\theta_g)\left(\frac{\pi G k_y}{2A^2}\right)(1+\tau^2)^{1/2} , \tag{25), (26}$$

where κ is the local epicyclic frequency. These are symmetric in terms of stars and gas ($i = s$ and g), as expected, since here stars and gas have been treated on an equal basis. The terms in the square brackets on the left-hand side arise, respectively, due to the epicyclic motion, the unperturbed shear flow in the disk, and the fluid pressure. The right-hand side denotes the self-gravity of the joint two-fluid system.

The schematic behavior of θ_i with τ is obtained by considering the evolution of a mode from a leading ($\tau < 0$, $|\tau|$ large), through a radial ($\tau \sim 0$), to a trailing position ($\tau > 0$, $|\tau|$ large). At large $|\tau|$ values, the pressure term dominates, and the solution for θ_i is oscillatory with a constant amplitude, and a frequency proportional to $c_i\tau$. This frequency is higher for stars than for gas since $c_s > c_g$. For large $|\tau|$, the two equations are weakly coupled. As the mode evolves from a leading to a radial position ($\tau \sim 0$), the terms denoting epicyclic motion and shear become important, and they nearly cancel each other. Hence these two effects are in a rough resonance for all realistic rotation laws, with the cancellation being total for a flat rotation curve. In addition, if the self-gravity dominates over the pressure term, then the mode undergoes swing amplification, that is, θ_i increases as it evolves from $\tau = 0$ to $\tau > 0$, i.e., from a radial to a trailing position—as explained by GLB, and Toomre (1981). The swing amplification is temporary—at large $\tau \gg 0$, the pressure term dominates and the solution is oscillatory again, assuming of course that we are in the linear regime at all times.

The maximum acceleration $[(d^2\theta_i/d\tau^2)/\theta_i]$ occurs at $\tau = 0$, as can be seen by setting $\mu_{0g} \to 0$ in equation (25). The maximum value of θ_i, $(\theta_i)_{\max}$, however, is reached later when the wave is trailing. Define maximum amplification factor (MAF) for a given mode as follows:

$$(\text{MAF})_i \equiv (\theta_i)_{\max}/(\theta_i)_{\text{ini}} , \tag{27), (28}$$

where $(\theta_i)_{\text{ini}}$ is the initial amplitude of oscillation of θ_i.

The coupling between the two fluids is highest at low $|\tau|$ values, exactly the region where amplification occurs. Hence, both θ_i and $(\theta_i)_{\max}$ in a two-fluid case are affected due to the presence of the other fluid.

Note that equations (25)–(26) describe two coupled oscillators, with time-dependent coefficients. Thus, the two-fluid system is capable of diverse, and complex behavior depending on the relative strengths of the two "natural frequencies" and the coupling constants.

In the nonaxisymmetric case, the ratio θ_s/θ_g varies with time in the sheared frame. In contrast, for the axisymmetric case, the equations governing the growth of two-fluid perturbations have no terms with time-dependent coefficients and hence these could be Fourier-analyzed in time, thus giving a constant value for the ratio $\delta\mu_g/\delta\mu_s$ (see JS1, their eq. [35]).

© American Astronomical Society • Provided by the NASA Astrophysics Data System

1992ApJ...390..378J

2.3. *Limiting Cases and Comparison with Earlier Work*

As an intermediate step to obtaining equation (25) from equations (15), (17), (19), and (22), we obtain a relation that is identical to equation (65) of GLB except for the difference in geometry; that is, $\delta\mu_s/\mu_{0s}$ is shown to be a linear function of v_{xs} and v_{ys}. Hence it follows that $\delta\mu_s \to 0$, in the limit of $\mu_{0s} \to 0$, for arbitrary values of v_{xs} and v_{ys}. Similarly, we also get a relation as in equation (66) of GLB, from which it follows that $[\partial(\delta\mu_s)/\partial\tau] \to 0$, when $\mu_{0s} \to 0$. Thus, in this limit, both the sides of equation (25) are identically equal to zero, for arbitrary $\delta\mu_g$. Therefore, in the limit of $\mu_{0s} \to 0$, the evolution of θ_g with τ is fully governed only by equation (26), which reduces to:

$$\left(\frac{d^2\theta_g}{d\tau^2}\right) - \left(\frac{d\theta_g}{d\tau}\right)\left(\frac{2\tau}{1+\tau^2}\right) + \theta_g\left[\frac{\kappa^2}{4A^2} + \frac{2B/A}{1+\tau^2} + \frac{k_y^2 c_g^2}{4A^2}(1+\tau^2) - \mu_{0g}\left(\frac{\pi G k_y}{2A^2}\right)(1+\tau^2)^{1/2}\right] = 0 . \quad (29)$$

This is identical to the corresponding equation for the non-axisymmetric perturbations in the one-fluid gas case (see eq. [72] of GLB) as expected, except for the term denoting self-gravity which is slightly different due to the thin disk assumption in our calculation.

In the other limiting case of $k_y \to 0$, that is when the perturbation wavevector is purely radial, equations (25)–(26) governing the evolution of θ_i with τ reduce to the dispersion relation for the two-fluid axisymmetric case obtained by JS1, as expected—the details are given in the Appendix.

3. RESULTS

3.1. *Solutions to the Perturbation Equations*

3.1.1. *Dimensionless Parameters*

We define the set of five dimensionless parameters Q_s, Q_g, ϵ, η, and X:

$$Q_s \equiv \frac{\kappa c_s}{\pi G\mu_{0s}}, \quad Q_g \equiv \frac{\kappa c_g}{\pi G\mu_{0g}}, \quad \epsilon \equiv \frac{\mu_{0g}}{(\mu_{0g}+\mu_{0s})}, \quad \eta \equiv \frac{2A}{\Omega_0}, \quad (30)$$

and

$$X \equiv \frac{\lambda_y}{\lambda_{\rm crit}},$$

where $\lambda_{\rm crit} = 4\pi^2 G(\mu_{0s}+\mu_{0g})/\kappa^2$.

Here Q_s and Q_g are the standard Q-factors (Toomre 1964) in the axisymmetric, local stability criterion for a one-fluid disk—for stars and gas, respectively. $Q > 1$ denotes stability and vice-versa. ϵ is the gas mass fraction in the galactic disk. η is the logarithmic shearing rate ($-[R_0/\Omega_0][d\Omega/dR]_0$) in the galactic disk. X is the wavelength of perturbation written in terms of $\lambda_{\rm crit}$, the critical wavelength for growth of instabilities in a one-fluid disk supported purely by rotation, with a surface density equal to the total disk surface density. This choice of $\lambda_{\rm crit}$ is used because the maximum growth occurs at low $|\tau|$, where the shear term dominates over the pressure term (eqs. [25]–[26]).

Thus, the ratio of the velocity dispersion in gas to that in the stars is given by

$$\frac{c_g}{c_s} = \frac{Q_g\epsilon}{Q_s(1-\epsilon)} . \quad (31)$$

Since the gas is the colder component, this ratio is always less than 1 in the present two-fluid analysis. This condition must be satisfied by any choice of values for Q_s, Q_g, and ϵ that are used to solve equations (25)–(26).

Note that the equation (30) defines a complete and single-valued set of dimensionless parameters for the current problem. This choice is suggested by the earlier work on the two-fluid axisymmetric case (JS2), and the one-fluid non-axisymmetric case (Toomre 1981). The above choice also facilitates a comparison of results from the present work with the results from these earlier studies; see § 3.2 for details.

In terms of the set of parameters as defined in the equation (30), the equations (25)–(26) describing evolution with τ in θ_i reduce to

$$\left(\frac{d^2\theta_s}{d\tau^2}\right) - \left(\frac{d\theta_s}{d\tau}\right)\left(\frac{2\tau}{1+\tau^2}\right) + \theta_s\left[\xi^2 + \frac{2(\eta-2)}{\eta(1+\tau^2)} + \frac{(1+\tau^2)Q_s^2(1-\epsilon)^2\xi^2}{4X^2}\right] = \frac{\xi^2}{X}(1+\tau^2)^{1/2}[\theta_s(1-\epsilon)+\theta_g\epsilon] \quad (32)$$

$$\left(\frac{d^2\theta_g}{d\tau^2}\right) - \left(\frac{d\theta_g}{d\tau}\right)\left(\frac{2\tau}{1+\tau^2}\right) + \theta_g\left[\xi^2 + \frac{2(\eta-2)}{\eta(1+\tau^2)} + \frac{(1+\tau^2)Q_g^2\epsilon^2\xi^2}{4X^2}\right] = \frac{\xi^2}{X}(1+\tau^2)^{1/2}[\theta_s(1-\epsilon)+\theta_g\epsilon] , \quad (33)$$

where $\xi^2 = \kappa^2/4A^2 = 2(2-\eta)/\eta^2$.

We solve equations (32)–(33) for the special case when the two-fluid system is stable against the growth of axisymmetric perturbations; this is analogous to the condition that Q be > 1 as used for the one-fluid case by Toomre (1981). This restriction allows us to obtain results for purely temporary growth in the surface densities as given by swing amplification (in the linear regime).

The condition that a two-fluid system is unstable to the growth of an axisymmetric perturbation was given by JS1 (see their eq. [22]). From this the condition for axisymmetric stability, in terms of the parameters in equation (30), is

$$\frac{(1-\epsilon)}{X'\{1+[Q_s^2(1-\epsilon)^2/4X'^2]\}} + \frac{\epsilon}{X'[1+(Q_g^2\epsilon^2/4X'^2)]} < 1 \quad (34)$$

where $X' = \lambda_a/\lambda_{\rm crit}$, with λ_a being the wavelength of the axisymmetric perturbation.

For every set of parameters (eq. [30]) used to solve the equations (32)–(33), we check that the above condition for stability is satisfied for all wavelengths (X') between $Q_g^2\epsilon/2$ to $Q_s^2(1-\epsilon)/2$. These correspond to the most unstable wavenumbers for gas and stars, respectively, and the wavenumber corresponding to the most unstable two-fluid perturbation lies in this range (JS1). A complete analysis of the parameter range for which a two-fluid system is stable against axisymmetric perturbations will be presented elsewhere (Jog 1992.

3.1.2. *Numerical Solutions*

In this section, we describe the details involved in obtaining numerical solutions of equations (32)–(33). These are two coupled, second-order, linear differential equations in θ_s and θ_g. We solve these by treating them as four coupled, first-order, linear differential equations in θ_s, $d\theta_s/d\tau$, θ_g, and $d\theta_g/d\tau$. These

© American Astronomical Society • Provided by the NASA Astrophysics Data System

1992ApJ...390..378J

are solved numerically by the fourth-order Runge-Kutta method with the given initial values at τ_{ini}, the initial value of τ (e.g., Press et al. 1986). The complete set of all possible initial values for these four variables is (1, 0, 0, 0), (0, 1, 0, 0), (0, 0, 1, 0), (0, 0, 0, 1), analogous to the choice (1, 0) and (0, 1) for the one-fluid case (GLB).

The resulting values of $(\theta_i)_{max}$ and the MAFs depend sensitively on the value of τ_{ini}, since the arrival phase at $\tau = 0$ is set by the choice for τ_{ini}. We thus optimize the value of τ_{ini} so as to obtain the highest possible values for the MAFs. This is identical to the approach used by Toomre (1981) for the one-fluid case. In a sense, therefore, the values of $(\theta_i)_{max}$ and MAF obtained in § 3.2 are stylized values. Using the optimal τ_{ini} as done here is probably reasonable for the local perturbations. In the optimization process one assumes that all perturbations with the above four sets of initial values are equally probable, and for each of these, all values of τ_{ini} are equally likely. Then given this spectrum of allowed initial perturbations, only the one showing the highest values of MAFs will dominate in a real two-fluid galactic disk. For the global case (not treated here), such an optimization cannot be assumed for all radial and azimuthal locations in a disk. Instead, one then needs to consider a wavepacket evolution as in Toomre (1969), and Goldreich & Tremaine (1978) (S. Tremaine, private communication).

In the local case presented in this paper, the optimal τ_{ini} turns out to be the same for gas and stars. This is not surprising, given the strong coupling between the two fluids at low values of τ. This is fortunate as it allows us to treat *coeval perturbations* in the two fluids.

We first check that for $\epsilon \to 0$, we obtain a plot of MAF for stars versus X for different values of Q_s that agrees with the corresponding plot (GLB with the Lin-Shu-Kalnajs reduction factor) in Figure 7 of Toomre (1981). We get somewhat smaller values of amplification since our choice of isothermal equation of state is stiffer. This plot is not given here as it does not lead to any new insight. Moreover, this agreement is expected from the first limiting case considered in § 2.3.

3.2. *Results for Swing Amplification in Stars and Gas*

In this section we present the results for swing amplification of nonaxisymmetric perturbations in the coupled stellar and gaseous fluids in a differentially rotating galactic disk. A vast range of values is available for the input parameters (eq. [30]). We choose realistic values for Q_s (Lewis & Freeman 1989), Q_g, and ϵ, the gas fraction (e.g., JS1). These are based on the observations of the Galaxy, covering a range from ~ 5 kpc (the peak of the molecular ring) to 8.5 kpc (the solar neighborhood)—see Scoville & Sanders (1987) for a radial distribution of gas in the Galaxy. These choices allow us to explore the two-fluid swing amplification in *dynamically distinct* cases. The values of input parameters are accurate only up to a factor of ~ 1 due to the observational uncertainties, plus the reduction in the effective surface density due to the finite disk height (e.g., JS1), and the use of total disk surface density instead of μ_{0s} by Lewis & Freeman (1989) in their estimates of Q_s values. However, we believe that the values used do represent realistic trends seen in the various regions of spiral galaxies.

We ensure that for each choice of Q_s, Q_g, and ϵ used, the condition of two-fluid axisymmetric stability (eq. [34]) is satisfied; and that the ratio c_g/c_s (eq. [31]) is < 1. We assume a flat rotation curve, as seen over the major portion of disks of most spiral galaxies, e.g., Bosma (1978) or Rubin, Ford, & Thonnard (1978). Hence, set $\eta = 1$, and $\xi^2 = 2$ in equations (32)–(33). The variation with η is given in § 3.2.3.

3.2.1. *Dependence on Q_s, Q_g, and ϵ*

We first consider the two-fluid results for various Q_s, Q_g, and ϵ values. Due to the observed values of parameters used, this also allows us to study the variation with radius in the Galaxy.

First, consider a typical case which illustrates the basic features of two-fluid swing amplification. The parameters as typical for the solar neighborhood are chosen. We set $Q_s = 1.5$ (Lewis & Freeman 1989), $Q_g = 1.5$, $\epsilon = 0.1$ (JS1, see their Appendix A), and $X = 1$. Figure 1 shows the resulting variation with τ in θ_s and θ_g, the dimensionless perturbation surface densities in stars and gas, obtained using the procedure described in § 3.1.2. The physical explanation for the schematic behavior of θ_i versus τ was given in § 2.2. The epoch of amplification in the sheared frame corresponds to the pitch angle in the uniformly rotating frame (§ 2.2). For the linear analysis given here, θ_i may be multiplied by an arbitrary scale factor α such that the net amplitude $\alpha\theta_i$ is $\ll 1$ at all τ.

The nonaxisymmetric perturbations show amplification (MAF > 1 in both fluids) even when the two-fluid system is stable to axisymmetric perturbations, as is indeed true of all the figures shown here. This is analogous to the one-fluid result by Toomre (1981).

The amplified spiral feature in gas shows a higher amplification (MAF), and it is also more tightly wound (i.e. has a higher pitch angle) than the stellar feature. Due to the lower gas velocity dispersion the pressure term allows growth in gas till a later epoch (eq. [33]) than in stars (eq. [32]), which leads to the above two results. The pitch angles at maximum growth for stars and gas are given by 69° and 76°, respectively. The net contrast, $\alpha\theta_{max}(\ll 1)$, is higher in gas than in stars as observed (e.g., Schweizer 1976; Young 1990). Some of the observed higher contrast in gas, however, could be due to nonlinear evolution of gas; we return to this issue in § 3.3. In order to compare the pitch angles in stars and gas, high-resolution CO

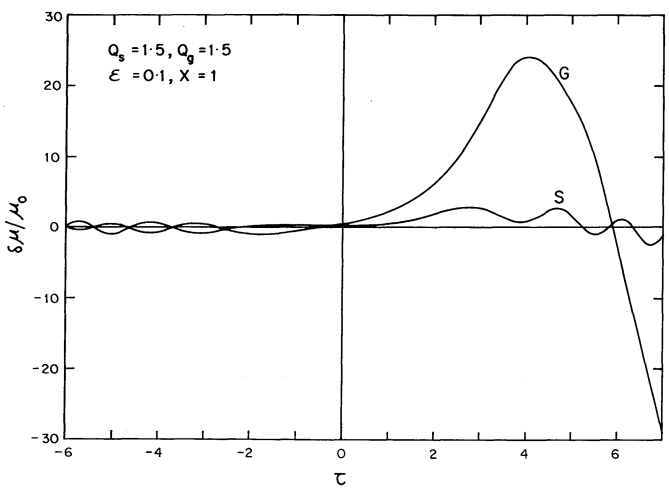

FIG. 1.—Variation in $\theta = \delta\mu/\mu_0$, the ratio of the perturbation surface density to the unperturbed surface density, with τ, the dimensionless time parameter in the sheared frame—for stars (curve S) and for gas (curve G). The parameters used are $Q_s = 1.5$, $Q_g = 1.5$, $\epsilon = 0.1$—as typical for the solar neighborhood region, and $X = 1$. The swing amplification in each fluid occurs at $\tau \geq 0$, as the perturbation swings past the radial position. The amplification is higher in the colder fluid, that is, gas, and the amplified gas feature is more tighly wound than the stellar feature. The net amplitude $\alpha\theta_i$ is $\ll 1$ at all τ, where α is a scale factor.

© American Astronomical Society • Provided by the NASA Astrophysics Data System

1992ApJ...390..378J

maps of galaxies need to be obtained—see, for example, the maps of M51 by Rand & Kulkarni (1990); and overlaid on the photometric maps or CCD images especially at long wavelengths. In M51, the CO spiral features do lie inside of the red continuum features representing arms in the old stellar populations (see Fig. 1*b* of Rand & Kulkarni 1990), as predicted from our analysis.

Next, consider the restrictive case when both the fluids are separately stable to the growth of nonaxisymmetric perturbations, a sufficient condition for this is that their respective Q-values be ≥ 2 (Toomre 1981; Carlberg & Freedman 1985; Larson 1988), while a smaller limit of $Q \geq 3^{1/2} = 1.7$ is given by Polyachenko (1989). Consider the set: $Q_s = 2$, $Q_g = 2$, $\epsilon = 0.1$, and $X = 1$. For these values, the gas in the two-fluid system shows amplification while the stars do not (the figure is not shown here). Evidently, even the small contribution by the hotter (stellar) component is sufficient to allow the colder component (gas) to show growth, while the converse is not true. This choice of parameters is typical for region around ~ 4 kpc, just inside of the peak of the molecular ring—here $Q_s = 2$ (Lewis & Freeman 1989), $Q_g = 2$, and $\epsilon = 0.1$ (JS1). This value of Q_g is obtained assuming c_g to be somewhat >5 km s^{-1}, because the gas velocity is robust and is expected to increase only slightly in the inner regions of the Galaxy (Jog & Ostriker 1988).

Next, consider a higher gas fraction, $\epsilon = 0.2$, and set $Q_s = 2$, $Q_g = 2$, and $X = 1$ (Fig. 2). Here *both the fluids in the two-fluid system show small but finite amplification even when both of them are separately stable* to the growth of nonaxisymmetric perturbations—this is possible because of the additional gravitational coupling between the two fluids, and the high fraction (20%) of disk mass in the cold fluid (gas). This is the nonaxisymmetric analog of the two-fluid axisymmetric result by JS1 (see their Figs. 4*a*–4*b*).

The parameters for Figure 2 may be typical of the outer regions of the disks of Magellanic-type irregular galaxies, which are characterized by κ and μ_t that are smaller by a factor of a few compared to a typical large spiral galaxy, while their

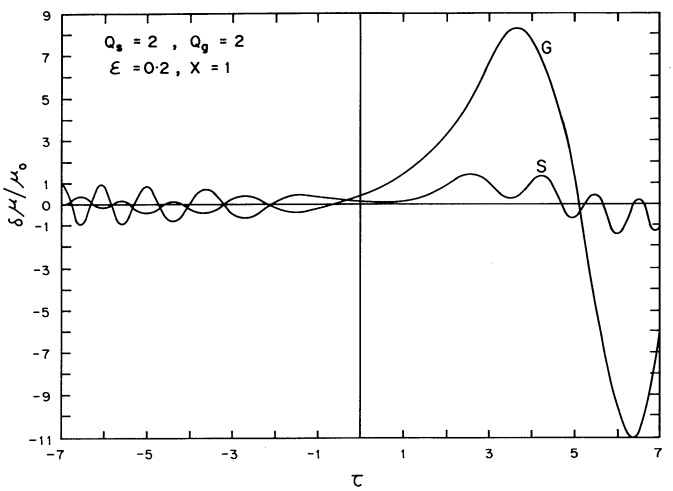

FIG. 2.—Variation in $\theta = \delta\mu/\mu_0$ with τ in stars (curve S) and in gas (curve G) for the parameters $Q_s = 2$, $Q_g = 2$, $\epsilon = 0.2$, and $X = 1$. Even when both the fluids are separately stable to the growth of nonaxisymmetric perturbations ($Q \geq 2$), the joint two-fluid system does show small but finite amplification. This is possible due to the gravitational interaction between the two fluids and a large fraction (20%) of mass in a cold fluid (gas).

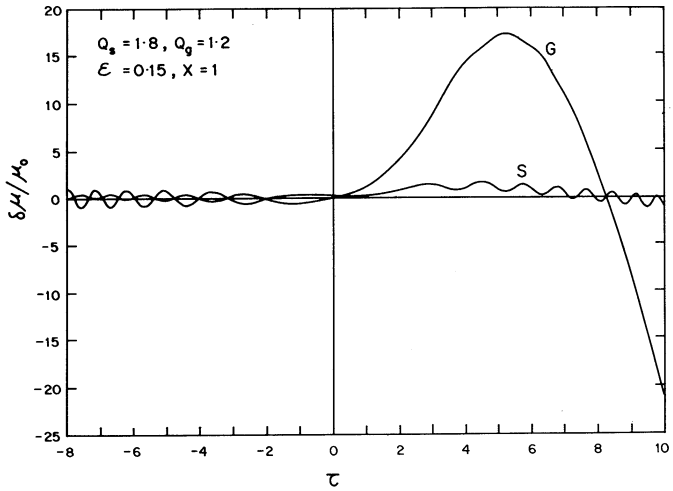

FIG. 3.—Variation in $\theta = \delta\mu/\mu_0$ with τ in stars (curve S) and in gas (curve G) for the parameters $Q_s = 1.8$, $Q_g = 1.2$, $\epsilon = 0.15$, as typical for the peak of the molecular ring region in the Galaxy, and $X = 1$. The high gas amplitude mainly determines the stellar curve, via the star-gas gravitational coupling. (The stellar pressure causes small oscillations about the positive mean, giving rise to a *scalloped* appearance of the stellar curve.) Here the range of pitch angles showing stellar growth is high. This results in the *broad stellar spiral arms*, discovered by Schweizer (1976). The arms are broader in the inner, gas-rich regions of a galaxy (compare with Fig. 1).

random velocities are similar to or even higher than in large spirals, and their gas fractions are high $\sim$20%–30% (e.g., Gallagher & Hunter 1984).

Next, we consider the other extreme case when the gas fraction is high and the gas by itself is close to being unstable to axisymmetric perturbations ($Q_g \rightarrow 1$), as for example is the case at the peak of the molecular ring in our Galaxy, and perhaps also for the central regions of other gas-rich galaxies. For this region at $r \sim 5$ kpc, the observed value of Q_s is $=1.8$ (Lewis & Freeman 1989), $Q_g = 1.2$, and $\epsilon = 0.15$ (JS1). We choose the higher value in the range for Q_g given by JS1 so that the condition for two-fluid axisymmetric stability (eq. [34]) is satisfied. The results are plotted in Figure 3 for $X = 1$. The MAFs are lower than in Figure 1. Because of the lower Q_g value, and the high gas fraction; the gas amplitude and hence the gas contribution to the self-gravity term is strong (see the right-hand sides of eqs. [32]–[33]). Hence, both stars and gas show fairly strong amplification in this case even though Q_s is high. Further, due to the lower $Q_g\,\epsilon$, the epoch of highest gas amplification occurs later than in Figures 1–2 (see the pressure term in eq. [33]). Hence, the gas feature is slightly more tightly wound, with a pitch angle of 79°.

In Figures 1–3, the stellar curve does oscillate at large τ as expected (§ 2.2), but it does so around a nonzero value, thus resulting in a *scalloped* appearance. This is a genuine physical effect and is due to the fact that when θ_g, the gas amplitude, and hence the gas contribution is high, it mainly determines the stellar curve via the star-gas coupling. Note that the mean of the scalloped distribution does mimic the gas curve. The stellar pressure term causes small oscillations around the mean positive value of θ_s, thus giving rise to the scalloping. The peak in θ_s though not sharply defined does occur earlier than for gas.

When the gas contribution is high, it increases the range of τ values (pitch angles) over which the stellar amplification can

© American Astronomical Society • Provided by the NASA Astrophysics Data System

1992ApJ...390..378J

occur. Our two-fluid scheme can, therefore, explain the *origin of the broad spiral arms/patterns* in the underlying old stellar populations as discovered by Schweizer (1976), and later seen in a larger sample by Elmegreen (1981) and Elmegreen & Elmegreen (1984). This is a major result from the present work. Note that, Schweizer's sample consists mainly of grand-design spiral galaxies; however, these also exhibit many local spiral features that may be explained as material arms as in our analysis. Elmegreen's sample contains many galaxies with a patchy, irregular spiral structure, for which our analysis is particularly applicable (§ 1).

We find that the stellar arms are broader in the inner, gas-rich regions of a typical spiral galaxy like the Galaxy (compare Figs. 1 and 3). We also predict the arms to be broader in gas-rich spiral galaxies. This is in fact seen for example in M33, NGC 6946, and NGC 2403 (see the *I*-band images in Elmegreen 1981)—these have very high gas fractions $\sim 25\%$ (e.g., Young 1990).

The narrowness of the blue arms (representing young stars) superposed on the broader, redder arms (representing older stars) as observed by Schweizer (1976) and Elmegreen (1981) could probably be explained by further nonlinear evolution of gas. Note that, in view of the dust extinction, far-infrared emission rather than the blue band emission or the Hα emission, may be a better tracer of the young, massive stars (e.g., Young et al. 1989).

In the extreme case when the gas contribution totally dominates, say for very high $\epsilon(>0.2)$, or very low $Q_g(<1.2)$, or when X is low; then the perturbations in gas and stars are found to remain in phase at all τ. Such cases are expected to be important in the early dynamical evolution of galaxies.

From Figures 1–3, and the discussion in this section, we conclude that strong amplification in (and coupling between) stars and gas will occur for moderate/small values of the Q-parameters (≤ 1.5), and for high gas fraction (~ 0.15–0.2). For our Galaxy, this corresponds to a range $r \sim 5$–8.5 kpc; and these parameters are probably typical of the intermediate radial regions of any spiral galaxy. The amplification is highest at the larger r values in this range, for both the stars and the gas. For a constant initial amplitude, $\alpha(\theta_i)_{\rm ini}(\ll 1)$, this implies a *radial increase of arm contrast*, $\alpha(\theta_i)_{\rm max}(\ll 1)$. This agrees with conclusions of Schweizer (1976) that the "fractional amplitudes of stellar patterns" [$\alpha(\theta_s)_{\rm max}$ in our notation], and the strength of star formation following gas amplification, both increase with radius. Schweizer's conclusions were based on the observations of radially increasing arm strengths (ratio of arm to disk intensity) in all wavelength bands. This trend has also been noted, though to a lesser degree, in the study by Elmegreen & Elmegreen (1984).

It is interesting that our linear analysis has allowed this comparison of our galaxy which has a ring distribution of gas, with results for Schweizer's sample—none of which show a ring distribution of gas (e.g., Young 1990; Kenney & Young 1989). If a lower and more realistic value of Q_g were to be used in the inner (ring) region, then the amplification would probably be strongest at the peak of the molecular ring and not in the outer region.

Finally, note that the Q-values are probably self-regulated, so that very large (>2) or small (<1.5) values of Q_s are not expected in a real spiral galaxy (GLB; Sellwood & Carlberg 1984). The observed values of Q_s for the Galaxy and for the few external galaxies for which data are available, do lie in the range of 1.5–2, except in the inner ~ 2 kpc region where higher values of Q_s are seen (Lewis & Freeman 1989; Kormendy 1984; van der Kruit & Freeman 1986; and Bottema 1989). Thus an upper bound of 2 for the Q_s values as used here seems reasonable.

3.2.2. *Dependence on X*

We next discuss the variation in results with X. Consider a lower X value = 0.5, for the solar neighborhood region, so that $Q_s = 1.5$, $Q_g = 1.5$, $\epsilon = 0.1$ (Fig. 4). Here the relative amplification in gas to that in the stars is higher than for $X = 1$ (see Fig. 1). The stellar curve again shows the scalloping effect indicating the dominance of gas contribution. The frequency of scalloping, which is set by the stellar pressure term (eq. [32]), is higher for the lower X value (compare Figs. 1 and 4), and also it is higher for a higher Q_s value for the same X (compare Figs. 1 and 3). Figure 4 shows that the two-fluid perturbations with $X < 1$ show significant growth unlike in the one-fluid case (Toomre 1981, Fig. 7). This is because of the amplification in gas for small X, which also affects the stars due to the gravitational coupling between the two fluids. Due to this coupling, ΔX, the range of wavelengths over which swing amplification occurs is extended for both gas and stars, to cover the purely gaseous case (low X) to purely stellar case (high X). This is analogous to the large range of unstable wavelengths seen for the two-fluid axisymmetric case, when ϵ is high and when $Q_g \sim 1$ (JS1, Figs. 4*c*–4*d*). The low-X modes would be dominant in gas-rich (late-type) galaxies.

Next, consider a larger X, say $X = 2$, and with the parameters as for the solar neighborhood (the figure is not shown here). Here the ratio of $(\theta_s)_{\rm max}$ to $(\theta_g)_{\rm max}$ is high $\sim 1/3$, as compared to $\sim 1/8$ for Figure 1. Interestingly, in this case, because of the higher relative θ_s and hence the higher stellar contribution (see eqs. [32]–[33]), it is the gas curve that shows modulation due to the stellar curve. This behavior would also be seen when $Q_s \sim 1$, except that such low values of Q_s are not realistic for galaxies at the present epoch. A detailed variation of two-fluid results with X will be presented in a future paper.

Finally, we check that for realistic values of parameters in spiral galaxies, the values of X in Figures 1–4 are in fact $\gg$ the

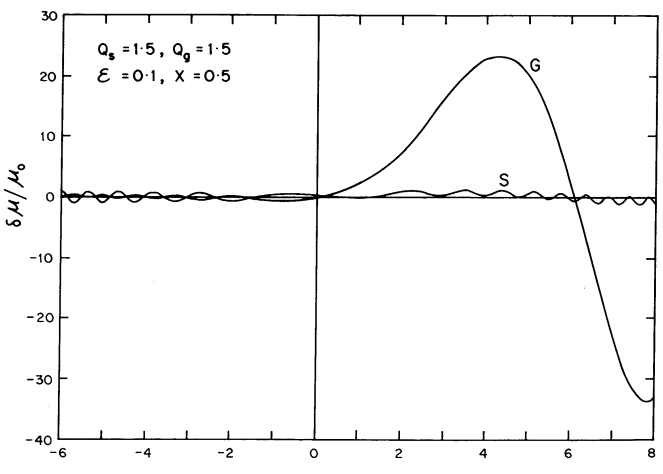

FIG. 4.—Variation in $\theta = \delta\mu/\mu_0$ with τ in stars (curve S) and in gas (curve G) for the same parameters as in Fig. 1, except now $X = 0.5$. The ratio of the amplification in gas to that in stars is higher than in Fig. 1. Note that, due to the coupling between the two fluids, both gas and stars show amplification even when X is < 1.

© American Astronomical Society • Provided by the NASA Astrophysics Data System

1992ApJ...390..378J

stellar scale height/λ_{crit} (see eq. [30]), as required for the thin disk approximation to be valid (§ 2.1).

3.2.3. *Dependence on η*

For a smaller shearing rate (η) than for a flat rotation curve as used here; the pressure term stops further growth at an earlier epoch (see eqs. [32]–[33])—thus resulting in more open features. This was pointed out by GLB and was verified numerically by Sellwood & Carlberg (1984) for Sc galaxies. Note that, this would also apply for the Magellanic-type dwarf irregulars since most of these show a slowly rising rotation curve in the outer regions (Casertano & Van Gorkom 1991). Conversely, a higher shearing rate—as is perhaps applicable for the early-type galaxies since they have a higher central concentration of mass (e.g., Bosma 1978), or the bright galaxies with falling rotation curves (Casertano & Van Gorkom 1991)—would lead to more tightly wound arms, as is seen for the early-type spiral galaxies.

The variation with gas fraction alone would tend to give an opposite trend, namely the mostly gas-rich, late-type galaxies would show more tightly wound arms. Clearly, the net variations in pitch angles depends on the combination of both these trends.

3.3. *Discussion*

In § 3.2, we could not explore the cases of the most virulent two-fluid amplification, say, when both Q-values are very low (<1.2) and/or the gas fraction is very high, $\epsilon > 0.2$, since the values of parameters used were restricted so as to satisfy equation (34) representing two-fluid axisymmetric stability. Such cases would be important for studying the early evolution of galaxies, or when a galaxy undergoes gas infall from outside which results in the lowering of Q_g values (Carlberg & Freedman 1985; Toomre 1990). These cases will be followed up in a future nonlinear analysis. Note that only a nonlinear analysis would yield values of $(\theta_s)_{max}$ and $(\theta_g)_{max}$ (with a scale factor $\alpha = 1$) that may be directly compared with the observations of surface density contrasts in spiral features in stars (Schweizer 1976) and in gas (e.g., Young 1990). Further, the recurrent formation of spiral features as sheared material arms following a nonlinear evolution, as proposed by GLB, is possible only in a two-fluid system. A nonlinear analysis may require the use of a collisionless representation of stars, since an isothermal fluid representation would give unrealistically large values of θ_s at large τ (Julian & Toomre 1966; also § 2.1). In a future paper, we will also discuss the global case.

In the present work, it has been assumed that all perturbations are equally probable (§ 3.1.2). In a real galaxy, and especially for the global case, the initial spectrum of perturbations may be decided by the presence of massive clouds in the galactic disk (Julian & Toomre 1966; Byrd, Smith, & Miller 1984; Toomre 1990), or by gas infall onto the galactic plane (Carlberg & Freedman 1985; Toomre 1990), or by a tidal interaction between galaxies. These would require a self-consistent treatment, not given here, for the perturber and the response to it (which in turn produces the perturber, i.e., a cloud, via nonlinear evolution).

It is observed that the arm contrast is smaller in galaxies with a patchy spiral structure than in the grand-design spiral galaxies (Elmegreen & Elmegreen 1984); the reason for this difference is not known. The global spiral patterns seen in the latter may be explained as density waves (Lin & Shu 1964; also see Binney & Tremaine 1987); however, in view of the high observed arm contrasts for these, the simple linear density wave picture is probably not applicable (Strom, Jenkins, & Strom 1976; Rand & Kulkarni 1990). Further, a galaxy may appear to be multiple-armed like M101 in the blue band, while it may appear as a grand-design spiral with a high arm contrast in the near-infrared (~ 1–2 μm), as seen in NGC 309 (Block & Wainscoat 1991). Even here, the local features seen in the blue band could be arising as material arms (§ 3.2) which could have a much lower contrast in red than the global pattern. Further high-sensitivity, multiband data are necessary to delineate this problem in more detail.

4. CONCLUSIONS

In summary, we have presented a study of the growth of local, nonaxisymmetric, linear perturbations in the coupled stars and gas in a differentially rotating galactic disk. We study the *physical effects of inclusion of a low velocity dispersion component (gas)* on the growth of perturbations in both stars and gas in a spiral galaxy.

The main results from this work are summarized below:

1. The amplification is higher in gas than in stars and the amplified gas spiral features are slightly more tightly wound than the stellar features. These results are due to the lower gas velocity dispersion, which allows a growth in gas till a later epoch in the sheared frame.

2. When the gas contribution is high, the stellar amplification and the range of pitch angles over which it can occur is also increased due to the gravitational coupling between the two fluids. Thus, the two-fluid scheme can explain *the origin of the broad stellar spiral arms* in the underlying old stellar populations of galaxies as observed by Schweizer (1976) and Elmegreen & Elmegreen (1984). This is a major result from the present work. The stellar arms are predicted to be broader in gas-rich galaxies, as is indeed seen for example in M33.

3. The input parameters as observed for the inner Galaxy (4–8.5 kpc) result in *radially increasing arm contrasts in old stars and gas*, which agrees with Schweizer's data (1976) for external galaxies. Our linear analysis has allowed this comparison of the Galaxy which has a ring distribution of gas, with the galaxies without rings as studied by Schweizer. If a lower Q_g value were to be used (which would require a nonlinear analysis), the amplification would then probably be highest at the ring region.

The above three results would be of even greater significance in future as the high spatial and spectral resolution photometric data from large single-dish telescopes and from optical and infrared interferometry become available for a large number of galaxies.

4. A real galaxy consisting of stars and gas may show growth of nonaxisymmetric perturbations even when it is stable against axisymmetric perturbations, and/or when either fluid is stable against nonaxisymmetric perturbations. The two-fluid system shows higher growth values than either fluid by itself, and also, the growth occurs over a larger range of wavelengths.

5. The two-fluid amplification process is expected to be important in the early dynamical evolution of galaxies, when the gas fraction would be much higher than at the present epoch. Here the two fluids evolve in phase at all times. This will be followed up in a future nonlinear analysis.

6. The analysis presented here, and the formulation of the

© American Astronomical Society • Provided by the NASA Astrophysics Data System

1992ApJ...390..378J

problem in terms of the five dimensionless parameters, is general and could be applied to other two-fluid disk systems—such as for example, the two-fluid accretion disks in active galactic nuclei (see Shlosman & Begelman 1989).

It is a great pleasure to thank J. P. Ostriker and S. Tremaine for many valuable discussions during the early stages of this work. I am grateful to J. P. Ostriker for his continued interest in this problem.

APPENDIX

THE TWO-FLUID NONAXISYMMETRIC CASE IN THE LIMIT OF $k_y \to 0$

We show that in the limit of k_y, the tangential wavenumber $\to 0$, that is when the perturbation wavevector is purely radial, equations (25)–(26) describing the evolution of two-fluid, nonaxisymmetric perturbations do reduce to the dispersion relation for the two-fluid axisymmetric case obtained by JS1.

We start with the general expression for τ (eq. [13]) and consider a general case when both the radial and the tangential wavenumbers k_x, $k_y \neq 0$. In the limit of $k_y \to 0$, the various functions of τ in equations (25)–(26) take on the following values: $1/(1+\tau^2) = 0$, $2\tau/(1+\tau^2) = 0$, and, $k_y(1+\tau^2)^{1/2} = k_x$.

Next, from the definition of τ it follows that for an arbitrary t:

$$2A \frac{d}{d\tau} = \frac{d}{dt} . \tag{35}$$

Thus in the limit of $k_y \to 0$, equations (25)–(26) simplify to the following

$$\frac{d^2\theta_s}{dt^2} + \theta_s(\kappa^2 + k_x^2 c_s^2 - 2\pi G k_x \mu_{0s}) = \theta_g 2\pi G k_x \mu_{0g} \tag{36}$$

$$\frac{d^2\theta_g}{dt^2} + \theta_g(\kappa^2 + k_x^2 c_g^2 - 2\pi G k_x \mu_{0g}) = \theta_s 2\pi G k_x \mu_{0s} . \tag{37}$$

These equations have no terms with coefficients involving time t and hence they can be Fourier-analyzed in time, say with a trial solution $\theta_s = \theta_{s0}[\exp(i\omega t)]$, and $\theta_g = \theta_{g0}[\exp(i\omega t)]$, where ω is the frequency of the perturbation. With this trial solution, equations (36)–(37) combine to give the following

$$(\omega^2 - \kappa^2 - k_x^2 c_s^2 + 2\pi G k_x \mu_{0s})(\omega^2 - \kappa^2 - k_x^2 c_g^2 + 2\pi G k_x \mu_{0g}) - (2\pi G k_x \mu_{0s})(2\pi G k_x \mu_{0g}) = 0 . \tag{38}$$

This is indeed identical to the dispersion relation obtained for a purely radial perturbation for the two-fluid axisymmetric case by JS1 (see their eq. [17]).

REFERENCES

Bertin, G. 1980, Phys. Rep., 61, 1
Binney, J., & Tremaine, S. 1987, Galactic Dynamics (Princeton: Princeton Univ. Press)
Block, D. L., & Wainscoat, R. J. 1991, Nature, 353, 48
Bosma, A. 1978, Ph.D. thesis, University of Groningen
Bottema, R. D. 1989, A&A, 221, 236
Byrd, G. G., Smith, B. F., & Miller, R. H. 1984, ApJ, 286, 62
Carlberg, R. G., & Freedman, W. L. 1985, ApJ, 298, 486
Casertano, S., & Van Gorkom, J. H. 1991, AJ, 101, 1231
Elmegreen, D. M. 1981, ApJS, 47, 229
Elmegreen, D. M., & Elmegreen, B. G. 1984, ApJS, 54, 127
Gallagher, J. S., & Hunter, D. A. 1984, ARA&A, 22, 37
Goldreich, P., & Lynden-Bell, D. 1965, MNRAS, 130, 125 (GLB)
Goldreich, P., & Tremaine, S. 1978, ApJ, 222, 850
Jog, C. J. 1992, in preparation
Jog, C. J., & Ostriker, J. P. 1988, ApJ, 328, 404
Jog, C. J., & Solomon, P. M. 1984a, ApJ, 276, 114 (JS1)
———. 1984b, ApJ, 276, 127 (JS2)
Julian, W. H., & Toomre, A. 1966, ApJ, 146, 810
Kenney, J. D. P., & Young, J. S. 1989, ApJ, 344, 171
Kormendy, J. 1984, ApJ, 286, 116
Larson, R. B. 1988, in Galactic and Extragalactic Star Formation, ed. R. E. Pudritz & M. Fich (Dordrecht: Reidel), 463
Lewis, J. R., & Freeman, K. C. 1989, AJ, 97, 139
Lin, C. C., & Shu, F. H. 1964, ApJ, 140, 646
Polyachenko, V. L. 1989, in Dynamics of Astrophysical Disks, ed. J. A. Sellwood (Cambridge: Cambridge Univ. Press), 199
Press, W. H., Flannery, B. P., Teukolsky, S. A., & Vetterling, W. T. 1986, Numerical Recipes (Cambridge: Cambridge Univ. Press), chap. 15
Rand, R. J., & Kulkarni, S. R. 1990, ApJ, 349, L43
Rubin, V. C., Ford, W. K., & Thonnard, N. 1978, ApJ, 225, L107
Schweizer, F. 1976, ApJS, 31, 313
Scoville, N. Z., & Sanders, D. B. 1987, in Interstellar Processes, ed. D. J. Hollenbach & H. A. Thronson (Dordrecht: Reidel), 21
Sellwood, J. A., & Carlberg, R. G. 1984, ApJ, 282, 61
Shlosman, I., & Begelman, M. C. 1989, ApJ, 341, 685
Strom, S. E., Jensen, E. B., & Strom, K. M. 1976, ApJ, 206, L11
Toomre, A. 1964, ApJ, 139, 1217
———. 1969, ApJ, 158, 899
———. 1981, in Structure and Dynamics of Normal Galaxies, ed. S. M. Fall & D. Lynden-Bell (Cambridge: Cambridge Univ. Press), 111
———. 1990, in Dynamics and Interactions of Galaxies, ed. R. Wielen (Berlin: Springer), 292
van der Kruit, P. C., & Freeman, K. C. 1986, ApJ, 303, 556
Young, J. S. 1990, in The Interstellar Medium in Galaxies, ed. H. A. Thronson & J. M. Shull (Dordrecht: Kluwer), 67
Young, J. S., Xie, S., Kenney, J. D. P., & Rice, W. L. 1989, ApJS, 70, 699

© American Astronomical Society • Provided by the NASA Astrophysics Data System